Giant Backscattering Magnetoresistance Resonance and Quantum Dot Electronic Structure

M. Stopa,* J. P. Bird, K. Ishibashi, Y. Aoyagi, and T. Sugano

RIKEN (The Institute of Physical and Chemical Research) 2-1, Hirosawa, Wako-Shi Saitama 351-01, Japan

(Received 14 December 1994; revised manuscript received 18 September 1995)

We self-consistently calculate in 3D the magnetic field dependent potential contour and semiclassical spectrum of a lateral quantum dot to analyze magnetotransport experiments. The spectrum differs dramatically from what had previously been assumed due to magnetically induced terraces in the potential. We show that a striking giant backscattering resonance in the data results from an increased Fermi level density of states associated with a terrace in the potential.

PACS numbers: 73.20.Dx, 73.40.Gk, 73.50.Jt

The introduction of self-consistency to the canonical picture of a two-dimensional electron gas (2DEG) in a transverse magnetic field B has recently led to a reinterpretation of the concept of edge states in the quantum Hall regime [1]. For sufficiently smooth potentials it is now recognized that the peculiar screening properties of electrons in a magnetic field lead to a breakup of the 2DEG into incompressible and compressible regions of integer and noninteger Landau level (LL) filling factors, ν, respectively. In compressible regions the Fermi energy E_F is pinned to a given Landau level, screening is good so the potential is flat or terrace shaped, and all the states of that Landau level are within k_BT of the Fermi surface. As a sample edge or potential hill is approached, compressible strips, separated by incompressible strips, have successively lower ν pinned to E_F, until a depletion region is reached.

It would be natural to expect transport anomalies in such a system which in the thermodynamic limit has a singular density of states (DOS) at the Fermi level. However, in the standard Hall bar configuration, the currents in *oppositely* propagating incompressible strips are widely separated on the scale of the magnetic length for typical B, thus effectively suppressing backscattering. In the case of a quantum dot having both adiabatically propagating and trapped edge channels, however, the singular DOS in a trapped "edge ring" can serve as a resonant path for electrons to backscatter between channels propagating *through* the dot in opposite directions. McEuen *et al.* [2], in an important study, introduced a self-consistent "addition spectrum" via a total energy functional into the study of magnetotransport through a small quantum dot in the *tunneling* regime. Nonetheless, some studies continue to ignore self-consistency in the potential altogether [3] while the so-called "Darwin-Fock" (DF) spectrum of an unrenormalized parabolic confining potential continues to form the basis of much analysis [4].

In this Letter we present results of experiment and calculation which show that, in an open lateral GaAs–AlGaAs quantum dot, the quasisingularities of the Fermi level DOS on terraces are a source of remarkable transport anomalies or "giant backscattering resonances." We perform full 3D self-consistent electronic structure calculations for our device using a Thomas-Fermi approximation modified to include magnetic field. From the B-dependent potential profiles we compute the semiclassical spectrum of the dot. The density of guiding center drift orbits in an edge ring and their location relative to the propagating channels permit an estimate, via an overlap matrix element, of the magnetic field trend of the coupling $t(B)$. The total coupling (summed over states) exhibits a pronounced maximum when electrons depopulate from higher LLs at the dot center, swelling the outer edge rings. Following Kirczenow [5] we model the transmission through the dot by ascribing unitary scattering matrices between edge channels at the dot corners nearest the quantum point contact (QPC) openings. Employing the computed $t(B)$ at all four assumed scattering locations we recover a resonance showing substructure similar to that which is experimentally observed and related to areas *between* the edge states. A fitting parameter, of the overall magnitude of t, is involved.

Dots were realized in a GaAs–AlGaAs wafer using a split-gate technique [6]. The wafer was patterned into a Hall bar with a carrier density $(3.5-4.4) \times 10^{11}$ cm^{-2}, and a mobility $35-40$ m^2/V s. Samples were mounted in a dilution refrigerator, and audio frequency magnetotransport measurements were made at fridge temperatures down to 10 mK. At high magnetic fields, the four-probe configuration employed was sensitive only to edge state transmission through the dot [7]. A source-drain voltage of less than 3 μV was employed.

Figure 1(a) shows the resistance R of a 1 μm square dot [cf. upper inset, Fig. 1(a)]. In the transition from two to one adiabatically transmitted edge channels, the fluctuation of the resistance around 3.5 ± 0.2 T results from an Aharanov-Bohm (AB) effect related to the area in a single QPC [6–8]. The resonant feature centered at 2.7 T, however, was not observed in single QPCs and appeared to be correlated with the depopulation of a bulk LL. Similar resonances, all robust with respect to thermal cycling, were also observed in other square dots of sizes 0.4, 0.6, 1.0, and 2.0 μm. The features were all coincident with bulk depopulations, although a resonance was not observed at *every* bulk depopulation.

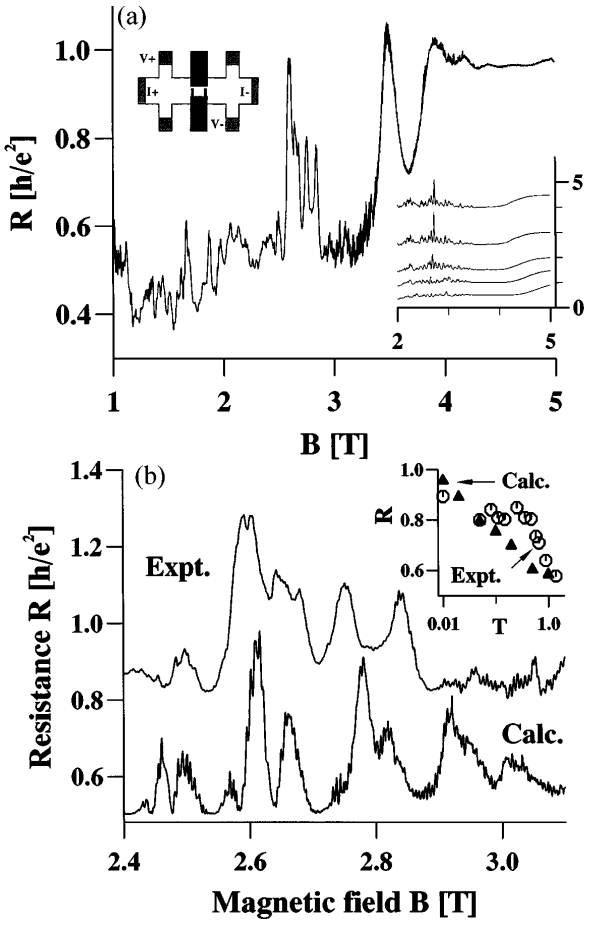

FIG. 1. (a) The magnetoresistance of a 1 μm quantum dot at 10 mK, showing giant magnetoresistance resonance near 2.7 T. Upper inset is device and measurement schematic. Lower inset shows gate voltage dependence of another 1 μm dot from a different wafer, from bottom $V_g = -0.415$, -0.419, -0.422, -0.424, and -0.436 V, vertically offset 0, 0.5, 1.0, 2.0, 4.0 h/e^2. (b) Expansion of resonant feature in 1(a) (above) and as calculated from Eq. (4). Experimental curve is offset for clarity. Inset shows peak resistance versus T [K] on log scale.

Further, they generally showed substructure, as with the resonance in Fig. 1(a), which is expanded in Fig. 1(b). Also, as shown in Fig. 1(a), lower inset, for a *different* 1 μm dot made from a different wafer with similar carrier concentration, the resonance generally becomes stronger with more negative gate voltage, suggesting that focusing by the QPC is enhancing scattering into higher LLs. This contrasts with the experiment of van Wees *et al.* [8] where the saddle point of the QPCs are only a small fraction of E_F above the potential floor of the ungated 2DEG regions. Thus in that experiment, when the second Landau level ($\lambda = 1$, see below) depopulates at the saddle, $\lambda = 2$ no longer exists in the dot as a possible resonant backscattering path.

The 3D electronic structure calculation has been described previously [9,10]. The essential modification here is the expression for the electron density in the magnetic field dependent Thomas-Fermi approximation [2,11,12]

$$n(x,y,z) = \frac{1}{2\pi\ell_c^2}\sum_{\lambda,s} f[(2\lambda+1)\mu_B^* B + g\mu_B B s + \varepsilon(x,y;B) - E_F]\,|\xi_{xy}(z)|^2\,, \tag{1}$$

where ℓ_c is the magnetic length, λ and s represent Landau level and spin, respectively, and $\mu_B^* \equiv e\hbar/2m^*c = (m_0/m^*)\mu_B$. $\xi_{xy}(z)$ and $\varepsilon(x,y;B)$ are the wave function and energy of the lowest z subband at x,y. The Fermi function and energy are f and E_F, and the Landé g factor is taken as the bare value for GaAs (-0.44). Note that, in contrast to Ref. [12], the calculation is fully 3D (there is no translationally invariant direction). For this device only the lowest z subband is occupied [9–11]. The results which we discuss here are based on self-consistent calculations carried out at $T = 100$ mK.

Figure 2 summarizes the evolution of the effective 2D potential contours with B. Potential is plotted as a function of *area A* of equipotential orbits about the dot center, $\varepsilon(A,B)$. The equipotential contours become nearly square at the Fermi surface and the terraces are therefore much wider in the corners. The total electron number in the dot is $N \approx 2800$ and varies (albeit in a complex fashion, peaking at around $B = 3$ T) by less than ± 4 electrons throughout. Thus, as the central terrace with $\lambda = 3$ ($\nu = 7, 8$) deepens with increasing B, shrinks in area, and depopulates altogether at $B \approx 3$ T, the lower λ terraces, particularly $\lambda = 2$, take up the $\lambda = 3$ electrons. Growth of $\lambda = 1$ is clearly visible and $\lambda = 0$, corresponding to the adiabatically propagating states, can just be discerned. A closer view of the region above 3 T (not shown) reveals spin split terraces for $\lambda = 2$ ($\nu = 5$ and 6).

Using the above $\varepsilon(A_m,B)$ for orbits whose area A_m intercepts m flux quanta, the semiclassical electronic *spectrum* is

$$E_{\lambda,m,s} = (2\lambda+1)\mu_B^* B + g\mu_B B s + \varepsilon(A_m,B)\,, \tag{2}$$

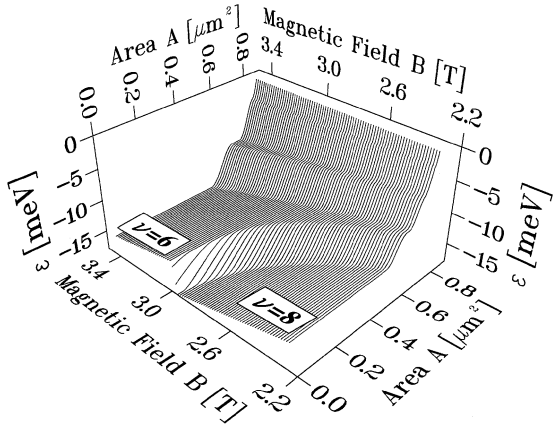

FIG. 2. Orbit potential as a function of the enclosed area and B. The $\nu = 7, 8$ terrace disappears abruptly at $B \approx 3$ T.

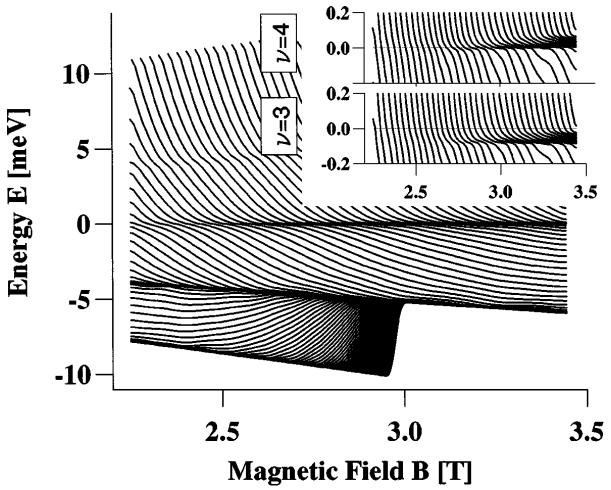

FIG. 3. Semiclassical spectrum of the $\nu = 4$ state as a function of B measured from the Fermi surface. Every 5th level plotted. Upper inset, expansion of spectrum near Fermi surface. Lower inset, spin-split state ($\nu = 3$) spectrum showing inflection occurring several $k_B T$ below the Fermi surface.

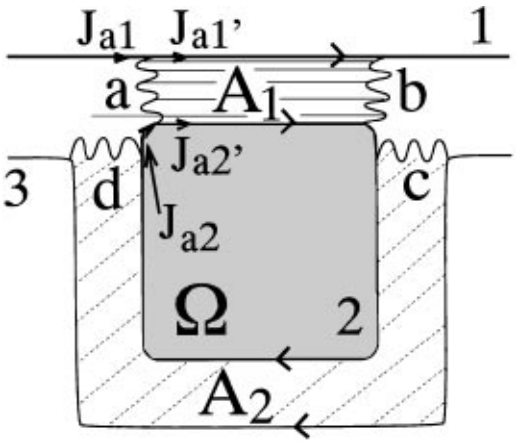

FIG. 4. Schematic illustrating calculation of backscattering from edge state 1, through confined edge ring 2 to edge state 3. Four identical scattering events (a)–(d) placed at ring corners. Currents incoming to scattering event a are J_{a1} and J_{a2}; outgoing are $J_{a1'}$ and $J_{a2'}$. Interedge state areas A_1 and A_2 greatly exaggerated with respect to trapped state area Ω.

which will be reasonable so long as higher order fluctuations in the potential are small over the length scale ℓ_c [13]. The spectra for the different ν differ only in their linear B dependence in the first two terms of Eq. (2). In Fig. 3, we plot the spectrum for the $\nu = 4$ states as a function of B. Dark regions of the spectrum and inflection lines reveal the presence of terraces. The disappearance of the central, $\lambda = 3$ terrace at $B \approx 3$ T is clearly seen by the sudden rise of all the low energy states (which are localized near the dot center). The two insets show the states of $\nu = 3$ and $\nu = 4$ within a few $k_B T$ of the Fermi surface. The inflection line for the $\nu = 4$ states are, in contrast to $\nu = 3$, right at the Fermi surface.

The terrace-induced enhancement of the $\nu = 4$ Fermi level DOS, in contrast to a single edge state at the Fermi surface as conceived in the standard Büttiker picture, makes possible a van Hove–like singularity in the inter-Landau level scattering. Following Kirczenow [5,14] we calculate R by placing discrete scattering events between propagating and trapped channels (Fig. 4). As noted previously, the terraces are widest near the dot corners. This combines with the known result [15] that inter-Landau level scattering is greatest where the edge channels bend most sharply. Thus we have coupled the free edge channels to the trapped channel only at the corners, as indicated. Each scattering event is characterized by a unitary, 2×2 matrix relating the two ingoing and two outgoing edge currents, for example:

$$\begin{pmatrix} r_a' & t_a \\ t_a & r_a \end{pmatrix} \begin{pmatrix} J_{a1} \\ J_{a2} \end{pmatrix} = \begin{pmatrix} J_{a1'} \\ J_{a2'} \end{pmatrix}, \tag{3}$$

where the J's are indicated in Fig. 4. We make the simplest possible assumption that all four scattering events are identical. Including the accumulated phases according to Ref. [5] and assuming weak scattering ($|t| \ll |r| \Rightarrow r \approx |r| \exp i\pi/2$) it is straightforward to derive the expression for the reflection coefficient of edge state ν through trapped state ν',

$$\mathcal{R}_{\nu,\nu'}(E,B) = \frac{4|t|^4|r|^4(1 + \cos A_1)(1 + \cos A_2)}{|1 - |r|^4 + |r|^2|t|^2[e^{i(\Omega + A_1)} + e^{i(\Omega + A_2)}] + |t|^4 e^{i(\Omega + A_1 + A_2)}|^2}. \tag{4}$$

Here $|r|^2 = 1 - |t|^2$ by unitarity. Ω, A_1, and A_2 are fluxes through corresponding areas labeled in Fig. 4; together with t they depend on ν, ν', E, and B and result from the self-consistent calculation. $\Omega_{\nu'}(E,B)$ can be determined directly from Fig. 2. A_1 and A_2 are determined from spacing between edge states. The sum $A_1 + A_2$ is taken to equal only 75% of the interedge state flux, so the scattering is not precisely at the corners. Coupling to inner ($\nu = 5-8$) states is negligible. So, assuming spin conservation, the dot resistance is calculated as

$$R^{-1}(B) = \frac{e^2}{h} \int dE \, \frac{df}{dE} [2 - \mathcal{R}_{1,3}(E,B) - \mathcal{R}_{2,4}(E,B)].$$

The calculated characteristic for $T = 50$ mK is shown in Fig. 1(b) beneath the expanded experimental trace. Note that when plotted on the same scale as Fig. 1(a), the calculated resistance peaks sharply near $B = 2.7$ T with no additional features. Structure in the peak results from

changing flux *between* LLs. When Ω is a multiple of 2π the leading term in Eq. (4) goes as $|t|^4[1 - \cos(A_1 + A_2)]$. The high B wing on the calculated resonance ($B \approx 2.95$ T) is absent from the experimental trace, implying that $t(B)$, which determines the overall shape, is more sharply peaked than our calculations indicate. Further, *AB* oscillations are observable in the experimental trace but are much more pronounced in the calculation. The action of the terraces can be thought of as broadening the *AB* peaks so that they overlap and produce the giant resonances. Additionally, broadening of the trapped levels via t, not included in the calculation, may smear the *AB* oscillations.

The position, approximate width, and internal structure of the calculated result agree remarkably well with experiment. Interestingly, the calculated resonant backscattering occurs in only one of two spin-split channels. $\mathcal{R}_{1,3}$ is almost uniformly negligible compared to $\mathcal{R}_{2,4}$. Separate terraces for $\nu = 3$ and 4 do not exist at this B. However, spin splitting is still much greater than k_BT. Thus only the $\nu = 4$ states are dense at the Fermi surface (cf. Fig. 3, inset) and serve to produce a van Hove–like backscattering anomaly. This behavior is consistent with one 1 μm dot sample [main part of Figs. 1(a) and 1(b)] where the resistance rises only to the next plateau. However, smaller dots (0.4 and 0.6 μm) and one *nominally identical* 1 μ*m dot* have shown resistance resonances which go *above* the next plateau (say from 0.5 h/e^2 to 20 h/e^2), implying backscattering of both spin species, $\nu = 1$ and 2.

Finally, the calculated temperature dependence of the peak resistance [Fig. 1(b), inset] differs appreciably from the observation. Experimentally, a clear threshold behavior out to $\sim$0.5 K (comparable to the bare spin splitting) is observed, beyond which the feature rapidly disappears. As noted earlier, the electronic structure is calculated at 100 mK. Therefores the calculated resistance depends on T only through df/dE. We repeated the self-consistent calculation at 0.5 K, however, but this appeared to have little effect on the characteristic, and the peak amplitude continued to fall well below the low temperature value and below experiment. We do not as yet have an explanation for this threshold behavior.

In conclusion, we have analyzed magnetotransport data using the evolving self-consistent electrostatic potential of a quantum dot. Within the semiclassical picture, the spectrum of a quantum dot is radically different from the normal Darwin-Fock–like spectrum which has served as the basis of conventional wisdom for many years. Inflection lines in the spectrum, which result from terraces in the magnetic field evolving potential, produce a significant increase in the Fermi surface density of states. This can cause a van Hove–like singularity in the Landau level coupling which leads to the experimentally observed giant backscattering resonances. An analysis of the transmission using the computed couplings and based on discrete scattering events at the dot corners accounts well for the resonant structure.

We wish to thank Holger F. Hofmann for helpful conversations. Computational support from the Fujitsu VPP500 Supercomputer in the Riken Computer Center is gratefully acknowledged.

*Electronic address: stopa@sisyphus.riken.go.jp

[1] D. B. Chklovskii, K. A. Matveev, and B. I. Shklovskii, Phys. Rev. B **47**, 12 605 (1993); A. M. Chang, Solid State Commun. **74**, 871 (1990); C. W. J. Beenakker, Phys. Rev. Lett. **64**, 216 (1990).

[2] P. L. McEuen, E. B. Foxman, J. Kinaret, U. Meirav, M. A. Kastner, N. S. Wingreen, and S. J. Wind, Phys. Rev. B **45**, 11 419 (1992).

[3] G. Kirczenow, A. S. Sachrajda, Y. Feng, R. P. Taylor, L. Henning, J. Wang, P. Zawadzki, and P. T. Coleridge, Phys. Rev. Lett. **72**, 2069 (1994).

[4] A. A. M. Staring, B. W. Alphenaar, H. van Houten, L. W. Molenkamp, O. J. A. Buyk, M. A. A. Mabesoone, and C. T. Foxon, Phys. Rev. B **46**, 12 869 (1992); R. C. Ashoori, H. L. Stormer, J. S. Weiner, L. N. Pfeiffer, K. W. Baldwin, and K. W. West, Phys. Rev. Lett. **71**, 613 (1993). In both of these publications the authors note clearly the possible shortcomings of the "constant interaction" model.

[5] G. Kirczenow, Phys. Rev. B **50**, 1649 (1994); G. Kirczenow and E. Castaño, *ibid.* **43**, 7343 (1991).

[6] J. P. Bird, K. Ishibashi, M. Stopa, R. P. Taylor, Y. Aoyagi, and T. Sugano, Phys. Rev. B **49**, 11 488 (1994).

[7] J. P. Bird, K. Ishibashi, Y. Aoyagi, T. Sugano, and Y. Ochiai, Phys. Rev. B **50**, 18 678 (1994).

[8] B. J. van Wees, L. P. Kouwenhoven, C. J. P. M. Harmans, J. G. Williamson, C. E. Timmering, M. E. I. Broekaart, C. T. Foxon, and J. J. Harris, Phys. Rev. Lett. **62**, 2523 (1989).

[9] M. Stopa, Y. Aoyagi, and T. Sugano, Surf. Sci. **305**, 571 (1994).

[10] M. Stopa, Phys. Rev. B **48**, 18 340 (1993).

[11] M. Stopa, J. P. Bird, K. Ishibashi, Y. Aoyagi, and T. Sugano, Superlattices Microstruct. **15**, 99 (1994).

[12] A similar approximation has been used recently in a 2D calculation for edge channel profiles by K. Lier and R. R. Gerhardts, Phys. Rev. B **50**, 7757 (1994).

[13] M. Tsukada, J. Phys. Soc. Jpn. **41**, 1466 (1976).

[14] M. Büttiker, IBM J. Res. Dev. **32**, 317 (1988).

[15] L. I. Glazman and M. Jonson, J. Phys. Condens. Matter **1** 5547 (1989).